Enhanced Lymph Vessel Density, Remodeling, and Inflammation Are Reflected by Gene Expression Signatures in Dermal Lymphatic Endothelial Cells in Type 2 Diabetes

Monika Haemmerle,[1] Thomas Keller,[1] Gerda Egger,[1] Helga Schachner,[1] Carl Walter Steiner,[2] Dejan Stokic,[3] Christoph Neumayer,[4] Markus K. Brown,[1] Dontscho Kerjaschki,[1] and Brigitte Hantusch[1]

Type 2 diabetes is associated with microvascular damage that causes frequent infections in the skin and chronic ulcers as a result of impaired wound healing. To trace the pathological changes, we performed a comprehensive analysis of lymphatic vessels in the skin of type 2 diabetic versus nondiabetic patients. The dermis revealed enhanced lymphatic vessel density, and transcriptional profiling of ex vivo isolated lymphatic endothelial cells (LECs) identified 160 genes differentially expressed between type 2 diabetic and nondiabetic LECs. Bioinformatic analysis of deregulated genes uncovered sets functionally related to inflammation, lymphatic vessel remodeling, lymphangiogenesis, and lipid and small molecule transport. Furthermore, we traced $CD68^+$ macrophage accumulation and concomitant upregulation of tumor necrosis factor-α (TNF-α) levels in type 2 diabetic skin. TNF-α treatment of LECs and its specific blockade in vitro reproduced differential regulation of a gene set that led to enhanced LEC mobility and macrophage attachment, which was mediated by the LEC-derived chemokine CXCL10. This study identifies lymph vessel gene signatures directly correlated with type 2 diabetes skin manifestations. In addition, we provide evidence for paracrine cross-talk fostering macrophage recruitment to LECs as one pathophysiological process that might contribute to aberrant lymphangiogenesis and persistent inflammation in the skin.
***Diabetes* 62:2509–2529, 2013**

The incidence of type 2 diabetes and obesity is rapidly increasing worldwide (1). Currently, generalized insulin insensitivity is considered the central pathogenic event (2) that is frequently linked to a systemic metabolic syndrome, a state of chronic low-level inflammation involving macrophage activation in adipose tissue (3). Recent insights also indicate genetic factors in the development of the disease (4). However, chronic hyperglycemia induces extensive macro- and microvascular alterations (5) that lead to systemic organ damage. Large vessels react to the chronically increased glucose and glucose-driven metabolites with enhanced arteriosclerosis. Diabetic microangiopathy gradually evokes retinopathy, leading to subsequent blindness, and nephropathy, the most frequent reason of renal insufficiency. In the skin, microvasculopathy causes prolonged inflammation, impaired healing of wounds, and ulcers (6).

Type 2 diabetes–induced microvascular lesions are characterized by aberrant matrix component deposition, resulting in narrowing of the vascular lumen that causes ischemia. Concurrently, the affected blood vessel endothelium shows imbalances of vasoconstrictors and -dilators, secretion of pro- and anti-inflammatory cytokines, and increased prothrombotic activity (7), which leads to leakiness and sustained effusion of leukocytes and plasma components into the tissue. In contrast to blood vessels, nothing is known so far about the involvement of the lymphatic vasculature in human type 2 diabetes, although dermal lymphatic vessels are known to play important roles in tissue fluid homeostasis, lipid absorption, and immune surveillance (8). Of note, lymphatic vessels function as collectors and export conduits of inflammatory cells, representing gatekeepers for macrophage and lymphocyte abundance in different tissues (9). Pathological processes of inflammation, wound healing, and adipogenesis, all relevant for type 2 diabetes, have been linked to functional defects of the lymphatic system in animal experiments (9). However, for human patients, it is currently unknown whether lymphatics remain unchanged, are passive bystanders, or participate actively in the skin lesions of type 2 diabetes.

In this article, we report on enhanced lymphatic microvessel density in the skin of type 2 diabetic patients. By comparing the gene expression profiles of freshly isolated dermal lymphatic endothelial cells (LECs) from patients with type 2 diabetes with those of normoglycemic controls, we identified molecular and cellular processes regulated in lymphatic vessels, in particular, proinflammatory, lymphangiogenic, and enhanced lipid shuttling properties, accompanied by downregulated immune defense, apoptosis mediators, and small compound transporters. Concomitantly, we traced a strong dermal $CD68^+$ macrophage infiltration, which elicited elevated tumor necrosis factor-α (TNF-α) levels. A subset of diabetic LEC (dLEC) deregulated genes was TNF-α responsive and correlated with lymphatic vessel remodeling and inflammation, including the chemokine CXCL10, which

From the [1]Clinical Institute of Pathology, Medical University of Vienna, Vienna, Austria; the [2]Department of Internal Medicine, Division of Rheumatology, Medical University of Vienna, Vienna, Austria; the [3]Section for Science of Complex Systems, Medical University of Vienna, Vienna, Austria; and the [4]Division of Vascular Surgery, Department of Surgery, Medical University of Vienna, Vienna, Austria.
Corresponding author: Brigitte Hantusch, brigitte.hantusch@meduniwien.ac.at.
Received 22 June 2012 and accepted 9 February 2013.
DOI: 10.2337/db12-0844
This article contains Supplementary Data online at http://diabetes.diabetesjournals.org/lookup/suppl/doi:10.2337/db12-0844/-/DC1.

specifically led to macrophage attraction and adhesion to LECs in vitro. Hence, we have obtained the first indications to our knowledge that the dermal lymphatic system is actively involved in the progression of skin manifestations in type 2 diabetes.

RESEARCH DESIGN AND METHODS

Skin samples from type 2 diabetic and nondiabetic patients. The study was approved by the local ethics committee (proposal no. 449/2001; 81/2008), and all patients (described in Supplementary Table 1) gave informed consent. Skin samples (n = 4 in each group) were taken from the proximal region of amputated legs or abdominoplastic tissue, and care was taken to excise areas at maximal distance from inflammatory or ulcerous changes (~15 cm).

Immunohistochemical analyses. Immunohistochemical stainings of paraffin-embedded or cryofixed skin sections were performed as described previously (10). Supplementary Table 2 summarizes the antibodies and respective dilutions applied. For quantifications, under exclusion of empty areas, non-overlapping microscopic fields (regions of interest [ROIs]) of 100 μm^2 (30 fields per patient) were captured with an Olympus VANOX AHBT3 microscope. Positively stained vessels, cellular nuclei, and macrophages were counted in these ROIs, and the cross-sectional dimension (referred to as diameter) of the vessels was measured. Average numbers were calculated per patient group and statistically analyzed as detailed later.

Ex vivo isolation of dermal LECs. Micropreparation of LECs was performed as described previously (10). Briefly, human skin was dermatomized and epidermis and dermis dislocated by incubation in dispase solution (Roche no. 04942086001). Cells were labeled with antibodies in a three-step procedure with intermediate washing steps and sorted (FACStar Plus; BD Biosciences, Franklin Lakes, NJ) as LECs ($CD31^+$ podoplanin positive) and blood endothelial cells ($CD31^+$ podoplanin negative) with the use of CD45 as a gate to exclude leukocytes.

RNA isolation and chip hybridization. GeneChip analysis was performed as described previously (10). Briefly, total RNA (RNeasy Mini Kit; Qiagen no. 74104) was amplified (MessageAmp II aRNA Amplification Kit; Ambion no. AM1751), and 1 μg of amplified RNA was biotin labeled, purified (MessageAmp II-Biotin Enhanced Kit, Ambion no. AM1791) and hybridized to Affymetrix GeneChips (GeneChip Human Genome U133 Plus 2.0 Arrays), which were scanned with GeneChip Scanner 3000 7G.

Bioinformatic data analysis. dLEC and nondiabetic LEC (ndLEC) gene expression profiles were analyzed with GeneSpring GX software (Ambion). After background correction, raw data were normalized with the robust multiarray average method, and P values were calculated by unpaired t testing. Subsequently, 1,828 probe sets with $P \leq 0.05$ were used for hierarchical clustering based on entities and conditions according to Euclidean distance metric and centroid linkage rules. All data have been deposited in the National Center for Biotechnology Information (NCBI) Gene Expression Omnibus (GEO) and are accessible through GEO accession number GSE38396 (http://www.ncbi.nlm.nih.gov/geo/query/acc.cgi?acc=GSE38396). Further in-depth bioinformatic analysis was performed by relative variance method (RVM), which allows for statistical analysis of small sample sizes based on a self-adaptive threshold (11). Extensive NCBI GEO and PubMed (http://www.ncbi.nlm.nih.gov/sites/entrez) research was amended to retrieve information on gene expressions and relevance for LEC biology. Gene ontology (www.affymetrix.com) was used to classify genes according to functionality. Ingenuity Pathway Analysis (http://www.ingenuity.com) was applied to identify associations with particular functions, canonical pathways, and diseases.

Quantitative reverse transcriptase–polymerase chain reaction. One microgram of amplified total RNA was transcribed into cDNA by Superscript II Reverse Transcriptase (Invitrogen no. 18064-014). A complete probe list is summarized in Supplementary Table 5.

Dermal LEC cultivation, TNF-α stimulation, and CXCL10 ELISA. LECs were sorted from human dermal microvascular endothelial cells (Promocell no. C-12260) by antipodoplanin antibody–coated magnetic beads. LECs were grown in endothelial basal medium-2 (EBM-2) supplemented with 5% FCS and EGM-2-MV SingleQuots (Lonza no. CC-4147) at 37°C and 5% CO_2. For TNF-α stimulations, LECs between passages 5 and 8 grown to 70–80% confluency in six-well plates were starved overnight in EBM-2/0.5% FCS and then medium containing 10 ng/mL TNF-α (R&D no. 210-TA-010) for 6, 12, and 24 h with or without 25 ng/mL inhibitory anti-TNF-α antibody was added. LECs were lyzed with RL buffer (Qiagen no. 79216) and β-mercaptoethanol for subsequent quantitative PCR (qPCR) analysis. LEC culture supernatants were collected and concentrated 20-fold with centrifugal filter units (Amicon Ultra-0.5 10K Ultracel R; Millipore no. UFC501024). Ninety-six-well ELISA plates were coated with concentrated supernatants overnight, and CXCL10 ELISA was performed according to standard protocol (see legend of Supplementary Fig. 8*B*). Experiments were performed in triplicate, and statistical differences between groups were analyzed as detailed later.

LEC motility and population doubling assay. For migration assay, a scratch wound was created in confluent LEC monolayers grown in 24-well plates. Nonadherent cells were washed away, fresh medium with or without TNF-α as described previously (n = 3) was added, and wound closure was monitored every hour with an inverted live cell microscope (Axiovert 200M; Zeiss). For population doubling analysis, identical LEC numbers were grown in six wells with or without addition of TNF-α (three in each group). After defined time points, cells were washed, trypsinized, and counted in a hemocytometer. Population doublings were calculated as ln(cell concentration counted/cell concentration seeded).

Macrophage adhesion and chemotaxis assay. Human monocytic leukemia cell line THP-1 (American Type Culture Collection no. TIB-202) was grown in RPMI 1640/10% FCS (Gibco no. 10108)/1% Pen/Strep and labeled with CellTracker Green CMFDA (5-chloromethylfluorescein diacetate) Molecular Probes 1:5,000 (Invitrogen no. C2925). Five by 10^5 cells were stimulated with 10 ng/mL phorbol myristic acid (PMA) (Sigma no. P8139) for 24 h, diluted in 500 μL EBM-2/0.5% FCS, and immediately added to LEC monolayers (n = 3). In blocking experiments, LECs were preincubated for 1 h with inhibitory anti-CXCL10 and anti-vascular cell adhesion molecule 1 (VCAM-1) antibodies before addition of THP-1 cells. After 3 h, nonadherent cells were washed away, and adherent THP-1 cells were photographed with an inverted live cell microscope (Axiovert 200M). Agarose spot assay was performed as described previously (12). Briefly, 1% agarose solution (Gibco no. 18300-012) was mixed 1:1 with concentrated LEC culture supernatants (see previous). Two 10-μL spots of this mixture were pipetted into 24-well plates and allowed to gel for 10 min at 4°C. Five by 10^5 THP-1 cells labeled and stimulated as described previously were added to each well. Inhibitory antibodies to TNF-α and CXCL10 were added 6 h before the end of the incubation period. After 24 and 48 h, images were taken, and the area covered by chemoattracted macrophages was measured with AxioVision version 4.7 software and plotted as the ratio of covered area to area at time 0.

Statistical analysis. Analyses were performed with Microsoft Excel 2007. Variance diversity of respective data sets was determined by the F test, and significance of difference was evaluated by Student t test. $P \leq 0.05$ was considered significant.

RESULTS

Enhanced lymphatic vessel density in type 2 diabetic skin. Immunohistological examination revealed thickened, laminin, and type IV collagen containing basement membranes of dermal blood vessels in type 2 diabetic patients (Fig. 1*A* and Supplementary Fig. 1*A*), which is characteristic for diabetic microangiopathy. Podoplanin-positive lymphatic vessels were devoid of laminin yet covered by type IV collagen in both groups (Fig. 1*A* and Supplementary Fig. 1*A*), indicating no changes in basement membrane composition. The average lymph vessel diameter was similar in both groups (not shown), suggesting an absence of lymphatic microvascular hyperplasia or edematous condition. Duffy antigen receptor for chemokines (13,14) was established as a distinct marker for blood vessel stainings of human skin sections (Supplementary Fig. 1*B*). In contrast to unaltered blood vessel counts, lymphatic vessel density was significantly increased in type 2 diabetes (1.8-fold, P = 0.035) (Fig. 1*B*). Moreover, whereas no Ki-67–positive nuclei were found in nondiabetic samples (Fig. 1*C*, arrowheads), 2% of nuclei (Fig. 1*C* and Supplementary Table 3) in podoplanin-positive lymphatic vessels expressed the proliferation marker Ki-67 in diabetic skin (Fig. 1*C*, arrows). Together, these data suggest that diabetic skin displays a higher lymphatic vessel density, which might be attributed to increased proliferation of LECs.

dLEC gene expression profile. To identify transcriptomal changes of lymphatic vessels in type 2 diabetes, we performed cDNA microarray analyses of ex vivo isolated dermal LECs (Supplementary Fig. 2) of four type 2 diabetic and four normoglycemic patients. Hierarchical clustering analysis of deregulated probe sets ($P \leq 0.05$)

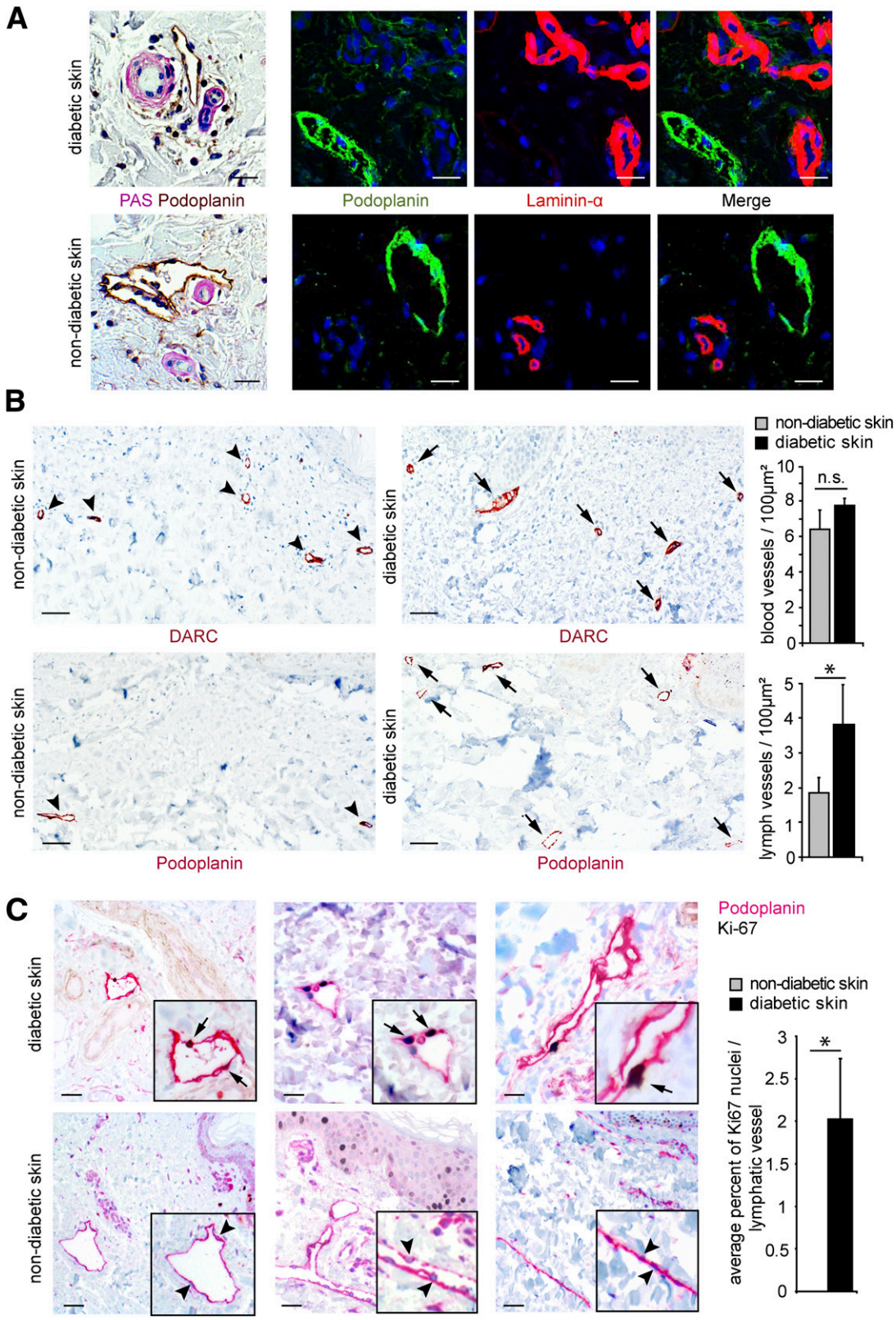

FIG. 1. Lymphatic vessel morphology, density, and proliferation in the skin of type 2 diabetic vs. nondiabetic patients. *A*: Paraffin sections of human type 2 diabetic and nondiabetic skin (n = 4 in each group) were double stained with periodic acid Schiff (PAS) (pink) and podoplanin (brown) to visualize glycoprotein deposits in basement membranes. PAS staining was prominent around diabetic blood vessels but absent from lymphatic vessels. Frozen sections of type 2 diabetic and nondiabetic human skin were double stained with antibodies to podoplanin (green) and the ECM protein laminin-α (red). Merged images show that laminin-α was absent from lymphatic vessels. Scale bars = 20 µm. *B*: Representative images and quantitative evaluation of immunohistochemical stainings of paraffin-embedded skin sections with antibodies to Duffy antigen receptor for chemokines for blood vessels and podoplanin for lymphatic vessels. Nonoverlapping fields (100 µm^2) of immunohistochemical stainings were captured and vessels counted within ROIs under omission of empty space. As indicated by arrows vs. arrowheads, in diabetic skin, blood vessel count was elevated 1.3-fold, but this was not significant (P = 0.7), whereas lymphatic vessel density was increased 1.75-fold (P = 0.035). Scale

revealed separation of dLEC and ndLEC samples into two groups (Fig. 2). Detailed statistical testing led to identification of the 160 top deregulated transcripts in dLECs, of which 38 were upregulated and 122 downregulated (Table 1). According to NCBI database screening, only 40% of the transcripts (63 genes) have been reported in LECs, lymph fluid, or both so far. Expression of established LEC identity markers was unchanged between dLECs and ndLECs (Supplementary Table 4), whereas deregulations of previously detected transcripts (10,15) indicated altered lymphatic properties in type 2 diabetes. Regulation of several genes (*HHEX*, *TSPAN8*, *LMNA*) (4) that were genetically linked to metabolic diseases showed that these markers prove valid in the lymphatic vessel compartment. Differential gene expression of selected gene candidates was confirmed by qPCR (Fig. 3*A*) and by immunofluorescence (Fig. 3*B* and *C*) at mRNA and protein levels, respectively (n = 4 per group). These findings revealed that ex vivo isolated LECs exhibit a distinct gene expression signature in type 2 diabetes.

Modulation of functional transcript groups in dLECs. To understand cellular processes associated with the dLEC transcript signature, we introduced a hierarchical categorization of the regulated genes on three levels. Gene ontology categories and manual annotation were used to assign basic functional descriptions to the genes, integrating these into distinct cellular process subgroups. Combined with Ingenuity Pathway Analysis (Supplementary Fig. 3), this led to the establishment of four overrepresented themes: *1*) defense response and inflammation, *2*) tissue remodeling and LEC motility, *3*) lymphangiogenesis and cell fate regulation, and *4*) lipid handling and small molecule biochemistry (Table 1). dLEC transcripts were highly enriched for plasma membrane (44 transcripts) and cell periphery and extracellular space (71 transcripts) (both $P < 0.001$, not shown), highlighting an extensive modulation at the environmental interface.

Altered defense and inflammation response of dLECs. Within gene cluster A (Table 1), established acute phase genes (*HP*, *PTX3*) and wounding factors (*NOX4*, *TXNL4B*) were upregulated, indicating an active reaction to injury signals, whereas expression of antimicrobial and defense response genes (*DEFB1*), inflammatory response genes (*PTGS2*, *PLA2G4A*), and immediate early genes (*CRIP1*) were downmodulated. Transcripts for chemotactic factors and leukocyte trafficking receptors (*CXCL10*, *VCAM1*, *CMTM7*) were enhanced, whereas several chemokines (*CCL27*, *CXCL14*, *STC1*), transcripts of interleukin-1 antagonists (*IL1R2*), and of anti-inflammatory interleukin signaling receptors (*IL20RB*, *IL13RA2*) were suppressed, pointing toward reduced signaling activation probably because of an enhanced cytokine milieu. Overall, the data show induction of certain acute phase, chemotactic, and stress response genes in dLECs, whereas several factors involved in the elimination of infections and inflammation are suppressed, suggesting a hampered anti-inflammatory response in dLECs.

Altered cell motility and morphogenesis of dLECs. Cluster B (Table 1) included a group of decreased transcripts for secreted growth factors (*CGA*, *AREG*), their carriers (*FGFBP1*, *IGFBP3*, *TGFBI*), and signaling components (*FGFR3*, *ANXA8L2*), indicating altered sensitivity to growth factor signals. Transcripts for extracellular matrix (ECM) degradation proteases (*TLL1*, *MMP2*) were induced, whereas their counterparts, proteinase regulators and inhibitors (*SERPINs*, *CAPNS2*), were suppressed, suggesting that dLECs actively pursue tissue degradation. Transcripts encoding integrin-binding and single-cell motility molecules (*CYR61*, *LYVE1*) were upregulated, whereas several transcripts for secreted proteoglycans (*SDC1*, *DCN*), ECM adhesion proteins (*GPNMB*, *CD44*), and filopodia formation proteins (*LY6D*, *IFFO2*, *ANK3*) were reduced, probably because of enhanced dLEC mobility. Well established was a group of decreased transcripts for cell-cell adhesion (*CXADR*, *CLDN1*) and desmosomal proteins (*DSC3*, *PKP1*, *DSG3*), pointing to altered mutual interaction between dLECs. The findings suggest that dLECs show a characteristic regulation of growth factor response, cell attachment, and adhesion transcripts, indicating overall ongoing lymphatic vessel remodeling.

Altered lymphangiogenesis and cell fate regulation of dLECs. Cluster C (Table 1) included transcripts coding for axon guidance factors (*NLGN4X*, *ROBO1*), suggesting phenotypic dLEC changes. Guanosine triphosphate enzyme (GTPase) activators (*RAPGEF2*, *RGS17*) were enhanced, whereas several small GTPase-associated transcripts (*RAB25*, *RND3*, *TAGAP*) were decreased, which might point toward sustained G-protein signaling during lymphangiogenic processes. A series of transcription factors were downmodulated, including transcriptional repressors (*BHLHB3*, *ID4*), regulators of proliferation (*HOPX*, *ID4*, *PER2*), and metabolism and cell growth *(FOXQ1*, *KLF5*, *TFAP2A*), many of these yet unknown in LECs except for the upregulation of *JUN* and *HHEX*, which foster cell growth and inflammation. Furthermore, downregulation of transcripts for promitotic (*TPPP3*, *ANLN*) and proapoptotic (*LGALS7B*, *P21*, *PERP*) factors suggested that dLECs reside in a postmitotic state accompanied by strong survival promotion. Overall, these findings suggest reactivated growth of dLECs. Importantly, the identified gene sets are in accordance with the initially observed enhanced lymphatic vessel density.

Altered lipid and small molecule handling of dLECs. Eminent within cluster D (Table 1) was upregulation of transendothelial lipid transport and handling molecules (*CYP46A1*, *FABP4*, *APOD*) and downregulation of enzymes involved in lipid oxidation and fatty acid degradation (*GPR109B*, *SCD-1*, *SLC27A2*), indicating increased influx and transport of free fatty acids by dLECs probably because of enhanced lipid status in the dermis of type 2 diabetic patients. Furthermore, transcripts for glucose (*SLC2A1*), amino acid (*SLC7A2*), water (*AQP3*), and chloride anion (*CLCA2*) transporters and for small compound metabolic enzymes (*KYNU*, *CA12*, *CPS1*) were decreased in dLECs, suggesting disturbed transport and biochemistry of small molecules.

Enhanced macrophage density and TNF-α levels in type 2 diabetic skin. To correlate the dLEC transcriptome with phenotypic changes of the skin, we performed bioinformatic pathway analyses to show enrichment

bars = 100 μm. *$P \leq 0.05$. *C*: Examples of lymphatic vessels in type 2 diabetic skin coexpressing podoplanin (pink) and nuclear proliferation marker Ki-67 (brown) in LECs and their quantification. An average 2% of LEC nuclei were positive for Ki-67 in diabetic skin (arrows), whereas no Ki-67–positive nuclei (arrowheads) were found in lymphatic vessels of nondiabetic skin ($P < 0.05$). Scale bars = 20 μm. *$P \leq 0.05$. NS, not significant.

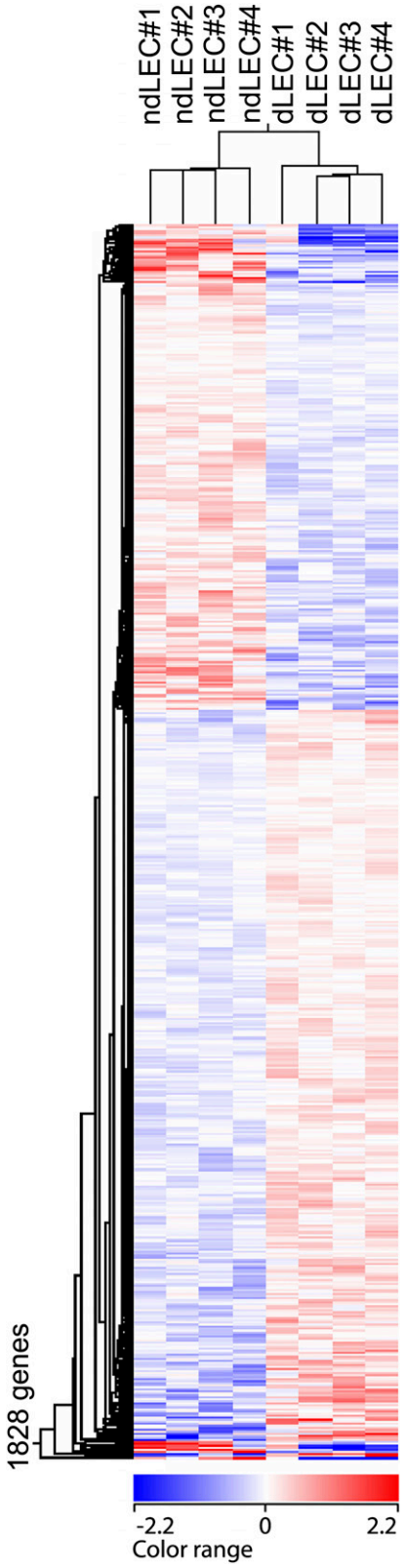

FIG. 2. dLECs exhibit a gene expression pattern separate from ndLECs. Hierarchical clustering of dLEC and ndLEC microarray gene expression data was based on 1,828 significantly deregulated probe sets shows grouping of dLECs and ndLECs in two separate branches. On the *y*-axis, an entity tree was generated by grouping the probe sets of the eight array samples according to the similarity of their expression profiles. On the *x*-axis, a condition tree was generated to show the relationship between the samples. The color range indicates the fold increased (red) and decreased (blue) expression difference of probe sets between dLECs and ndLECs.

of gene signatures related to immune response, inflammation, and leukocyte trafficking (Supplementary Fig. 4). As one mechanism for diabetic skin complications, the enhanced presence of alternatively activated macrophages was proposed (16). Hence, we explored immune cell abundance in the same skin samples used for LEC isolation. Although T-cell and dendritic cell counts were not significantly altered (not shown), we found a massive 3.5-fold increase ($P < 0.001$) of $CD68^+$ macrophages in type 2 diabetic skin (Fig. 4*A*). Growing evidence in the literature suggests insulin resistance as a result of a chronic inflammatory milieu (3) that involves macrophage-derived TNF-α as a prominent pathophysiological stimulus (17). After establishing TNF-α immunofluorescence stainings (Supplementary Fig. 5), type 2 diabetic skin revealed enhanced TNF-α abundance (Fig. 4*B*) and double immunofluorescence localized TNF-α expression to $CD68^+$ macrophages (Fig. 4*C*). Densitometric evaluation showed that 60% of these cells expressed TNF-α in diabetic skin but only 20% in nondiabetic skin (Fig. 4*D*), which denoted an additional threefold increase of TNF-α levels. Macrophage infiltration is a major driver of prolymphangiogenic processes by secretion of lymphangiogenic factors (18). We determined that 90% of the macrophages expressed vascular endothelial growth factor (VEGF)-C and VEGF-A in both skin subtypes (Supplementary Fig. 6), indicating moderately enhanced levels in type 2 diabetes because of enhanced macrophage levels. Essentially, we traced elevated TNF-α levels produced by macrophages that were extensively infiltrating the skin of type 2 diabetic patients.

TNF-α recapitulates dLEC gene expression changes and leads to enhanced LEC motility. To analyze whether the dLEC transcriptome mirrored enhanced interstitial TNF-α levels, we performed an in-depth analysis of data on LECs stimulated with TNF-α in vitro (19,20) (Supplementary References 1 and 2) and identified a gene set (*CXCL10*, *VCAM1*, *CYR61*, *AQP3*, *CXADR*, *SDC1*) that matched with the dLEC expression changes. Primary human dermal LECs were controlled for stable identity in vitro (Supplementary Fig. 7). Thereafter, TNF-α treatment recapitulated upregulation of *CYR61* and suppression of *AQP3*, *CXADR*, and *SDC1* transcripts, similar to ex vivo dLECs (Fig. 5*A*). Anti-TNF-α blocking antibody abolished respective up- and downregulation of the transcripts (Fig. 5*A*), confirming TNF-α–dependent gene regulation. We aimed to explore whether TNF-α–modulated gene expression changes had functional relevance in LECs. CYR61 is an ECM-associated protein that stimulates angiogenesis and vascular integrity (21), CXADR is a homophilic cell adhesion molecule essential for lymph vessel development (22), and SDC1 is a proteoglycan that modulates ECM binding (19). Hence, *CYR61* upregulation and *CXADR* and *SDC1* downregulation suggested reduced intercellular adhesion and enhanced migratory behavior of LECs. Area closure of scratch wounds in LEC monolayers occurred significantly faster under TNF-α treatment (Fig. 5*B*), which was not a result of increased cell population doublings because TNF-α–treated cells showed significantly lower doubling rates than untreated controls (Fig. 5*C*). These data suggest that TNF-α–mediated gene expression changes evoke a lymphatic vessel remodeling phenotype that depends on increased LEC motility.

TNF-α stimulates macrophage adhesion to LECs. *CXCL10* and *VCAM1* were the transcripts most strongly regulated by TNF-α. We confirmed TNF-α–mediated *CXCL10* and *VCAM1* upregulation in vitro, which was

TABLE 1
Transcript levels of 160 deregulated candidate genes functionally clustered in inflammatory response, LEC adhesion and migration, growth and lymphangiogenesis, and small molecule biochemistry

Affymetrix ID	Accession	Gene	Gene description	Ratio*	*P* value; RVM†	Molecule/function‡
Cluster A: inflammatory response						
Innate immune and acute phase response						
208470_s_at	NM_005143	*HP*	Haptoglobin	8.43	0.008	Peptidase, acute phase protein
206157_at	NM_02852	*PTX3*	Pentraxin-related gene	2.80	0.0003	Acute phase protein, regulation of innate immunity
200838_at	NM_001908	*CTSB*	Cathepsin B	1.78	0.006	Lysosomal cysteine peptidase, cellular stress and wounding, APP processing
200986_at	NM_000062	*SERPING1*	Serpin peptidase inhibitor, clade G (C1 inhibitor), member 1	1.71	0.005	Peptidase inhibitor, regulates complement component C1S
200602_at	NM_000484	*APP*	Amyloid precursor protein	1.54	0.039	Acute phase protein
205821_at	NM_7360	*KLRK1*	Killer cell lectin-like receptor subfamily K, member 1	0.23	RVM	MHCI receptor, innate immunity
208155_x_at	NM_001468	*GAGE1*	G antigen 1	0.23	RVM	Antigenic peptide, defense response
210397_at	U73945	*DEFB1*	Defensin, β 1	0.20	0.032	Antimicrobial peptide, defense response
218677_at	NM_020672	*S100A14*	S100 calcium binding protein A14	0.11	0.012	Ca^{2+} and RAGE ligand, chemotactic
219612_s_at	NM_000509	*FGG*	Fibrinogen γ chain	0.08	RVM	Fibrin monomer, inflammatory marker
204971_at	NM_005213	*CSTA*	Cystatin A	0.05	0.012	Cysteine protease inhibitor, regulates CTSB
Wounding and stress response						
236843_at	NM_001143836	*NOX4*	NADPH oxidase 4	4.81	0.041	Oxygen sensor, ROS production, inflammatory response
222748_s_at	AW194729	*TXNL4B*	Thioredoxin-like 4B	3.77	0.008	Spliceosomal protein, oxidative stress
203060_s_at	NM_004670	*PAPSS2*	3′-phosphoadenosine 5′-phosphosulfate synthase 2	3.27	0.030	ATP-binding enzyme, anti-inflammatory
200799_at	NM_005345	*HSPA1A*	Heat shock 70 kDa protein 1A	1.88	0.024	Protein folding enzyme, cell stress
210145_at	NM_024420	*PLA2G4A*	Phospholipase A2, group IVA (cytosolic, calcium dependent)	0.28	0.038	Arachidonic acid–releasing enzyme, proinflammatory
206461_x_at	NM_005951	*MT1H*	Metallothionein 1H	0.27	0.029	Zn-binding protein, antioxidant
204326_x_at	NM_002450	*MT1X*	Metallothionein 1X	0.23	RVM	Zn- and Ca-binding protein, ion homeostasis, antioxidant
217546_at	NM_176870	*MT1M*	Metallothionein 1M	0.19	0.008; RVM	Cu-, Zn-, Cd-binding, wound healing
205081_at	NM_001311	*CRIP1*	Cysteine-rich protein 1 (intestinal)	0.17	0.011; RVM	Zn finger protein family, immediate early gene

Continued on facing page

TABLE 1
Continued

Affymetrix ID	Accession	Gene	Gene description	Ratio*	*P* value; RVM†	Molecule/function‡
213506_at	BE965369	*F2RL1*	Coagulation factor II (thrombin) receptor-like 1	20.17	0.010; RVM	Receptor for trypsin and trypsin-like enzymes coupled to G proteins, innate immune response
204748_at	NM_000963	*PTGS2*	Prostaglandin G/H synthase and cyclooxygenase	0.17	0.002; RVM	Prostaglandin-producing enzyme, inflammatory mediator
230720_at	NM_001165032	*RNF182*	Ring finger protein 182	0.10	RVM	Ubiquitin ligase, MHCI-associated antigen processing
Chemotaxis, leukocyte adhesion and extravasation						
204533_at	NM_001565	*CXCL10*	Chemokine (C-X-C motif) ligand 10	5.16	RVM	Chemokine ligand, chemotactic for monocytes and T cells
203868_s_at	NM_001078	*VCAM1*	Vascular cell adhesion molecule-1	4.23	0.001; RVM	Integrin receptor, leukocyte adhesion molecule
226017_at	NM_138410	*CMTM7*	CKLF-like MARVEL transmembrane domain containing 7	1.52	0.030	Chemokine like, unknown function
205945_at	NM_000565	*IL6R*	Interleukin 6 receptor	0.30	RVM	Subunit of the interleukin 6 receptor complex
205403_at	NM_004633	*IL1R2*	Interleukin 1 receptor, type II	0.26	0.047; RVM	Cytokine decoy receptor
206172_at	NM_000640	*IL13RA2*	Interleukin 13 receptor, α 2	0.22	RVM	Chemokine receptor, suppresses T-cell response
204597_x_at	NM_003155	*STC1*	Stanniocalcin 1	0.21	0.017; RVM	Pleiotropic homodimeric glycoprotein, anti-inflammatory
222484_s_at	NM_004887	*CXCL14*	Chemokine (C-X-C motif) ligand 14	0.11	0.0005; RVM	Chemokine, acting on macrophages and DCs
228575_at	NM_144717	*IL20RB*	Interleukin 20 receptor β	0.11	0.049	Coreceptor for interleukin 20, suppresses T-cell response
207955_at	NM_006664	*CCL27*	Chemokine (C-C motif) ligand 27	0.06	0.006	T cell–attracting chemokine
Cluster B: LEC adhesion and migration						
Growth factors and signaling						
1554833_at	NM_018349	*MCTP2*	Multiple C2 domains, transmembrane 2	5.14	0.045	Ca binder in absence of phospholipids, Ca-mediated signaling
203819_s_at	NM_006547	*IGF2BP3*	Insulin-like growth factor 2 mRNA binding protein 3	0.28	RVM	mRNA binder, translational regulator of IGF-2, antiproliferative
206100_at	NM_001874	*CPM*	Carboxypeptidase M	0.27	RVM	Membrane peptidase, controls hormone and growth factor activity
201506_at	NM_000358	*TGFBI*	Transforming growth factor, β-induced, 68 kDa	0.23	0.006; RVM	Signaling molecule, cell-collagen interaction, inhibits cell adhesion

Continued on next page

TABLE 1
Continued

Affymetrix ID	Accession	Gene	Gene description	Ratio*	*P* value; RVM†	Molecule/function‡
210095_s_at	M31159	*IGFBP3*	Insulin-like growth factor binding protein 3	0.22	0.008	Carrier protein for IGFs, prolongs their half-life
209795_at	NM_001781.2	*CD69 = CLEC2*	CD69 molecule	0.20	RVM	Ca-dependent lectin superfamily of type II transmembrane receptors, signaling
225316_at	NM_032793	*MFSD2A*	Major facilitator superfamily domain containing 2	0.19	0.035	Multipass membrane protein, supposed tumor suppressor, antimigratory
205239_at	NM_001657	*AREG*	Amphiregulin	0.17	RVM	EGF-like autocrine growth factor, involved in growth and inflammation
204268_at	NM_005978	*S100A2*	S100 calcium binding protein A2	0.16	0.028; RVM	EF-hand Ca-binding protein, Ca-sensor involved in cell growth regulation
203638_s_at	NM_005130	*FGFBP1*	Fibroblast growth factor binding protein 1	0.11	0.025	Carrier protein that releases FGFs from the ECM
203074_at	NM_001630	*ANXA8L2*	Annexin A8-like 2	0.10	0.023	Ca-dependent phospholipid-binding, membrane organization signaling
204637_at	NM_000735.3	*CGA*	Glycoprotein hormones, α polypeptide	0.10	RVM	Hormone subunit, involved in vascularization, cell death, metabolism
204379_s_at	NM_000142	*FGFR3*	Fibroblast growth factor receptor 3	0.09	0.032	FGF signaling receptor influencing mitogenesis and differentiation
ECM proteolysis						
1555071_at	NM_012464	*TLL1*	Tolloid-like 1	2.36	0.042	Metalloprotease, regulates ECM formation
201069_at	NM_00453	*MMP2*	Matrix metallopeptidase 2	2.14	0.008	Type IV collagen degrading enzyme, vascular remodeling and tissue repair
204475_at	NM_002421	*MMP1*	Matrix metallopeptidase 1 (interstitial collagenase)	0.26	0.023; RVM	Collagenase, peptidoglycan metabolism
206421_s_at	NM_003784	*SERPINB7*	Serpin peptidase inhibitor, clade B (ovalbumin), member 7	0.24	RVM	Serine-type endopeptidase inhibitor
210715_s_at	NM_021102	*SPINT2*	Serine peptidase inhibitor, Kunitz type, 2	0.15	0.009	Serine-type protease inhibitor, inhibitor of HGF activator, controls cell motility
204489_s_at	NM_032330	*CAPNS2*	Calpain, small subunit 2	0.14	0.039	EF-hand, Ca-binding protein, regulatory unit for Ca-activated proteases
220051_at	NM_006799.2	*PRSS21*	Protease, serine, 21 (testisin)	0.14	RVM	Serine protease
204855_at	NM_002639	*SERPINB5*	Serpin peptidase inhibitor, clade B (ovalbumin), member 5	0.13	0.009; RVM	Serine-type endopeptidase inhibitor

Continued on facing page

TABLE 1
Continued

Affymetrix ID	Accession	Gene	Gene description	Ratio*	*P* value; RVM†	Molecule/function‡
204614_at	NM_002575	*SERPINB2 = PAI2*	Serpin peptidase inhibitor, clade B (ovalbumin), member 2	0.11	0.038; RVM	Serine-type endopeptidase inhibitor, uPA inhibitor
ECM adhesion/ cell migration						
236361_at	NM_054110	*GALNTL2*	UDP-N-acetyl-α-D-galactosamine: polypeptide N-acetylgalactosaminyl transferase-like 2	3.91	0.011; RVM	Glycosyltransferase catalyzing O-linked polysaccharide biosynthesis during developmental processes
220037_s_at	NM_006691	*LYVE1*	Lymphatic vessel endothelial hyaluronan receptor 1	2.50	0.036	Hyaluronic acid–binding type 1 membrane protein, cell motion, cell adhesion
221447_s_at	NM_031302	*GLT8D2*	Glycosyltransferase 8 domain containing 2	2.13	0.038	Glycosyltransferase, protein modification
210764_s_at	NM_001554	*CYR61*	Cysteine rich protein 61	2.09	0.020	ECM protein, interacts with integrins and heparan sulfate, proangiogenic
215446_s_at	NM_002317.5	*LOX*	Lysyl oxidase	2.00	0.007	Extracellular copper enzyme, initiates the cross-linking of collagens and elastin
205612_at	NM_007351	*MMRN1*	Multimerin 1	1.75	0.013	Elastin microfibril interfacer protein, integrin ligand
203066_at	NM_015892	*GALNAC4S-6ST*	Carbohydrate sulfotransferase 14	1.68	0.031	Glycosaminoglycan biosynthesis, ECM formation
210809_s_at	D13665	*POSTN*	Periostin, osteoblast specific factor	0.26	0.014	Member of the fasciclin family, heparin binding, induces cell attachment
212014_x_at	NM_000610	*CD44*	CD44 molecule	0.20	0.020; RVM	Hyaluronic acid receptor, regulates matrix adhesion and cell migration
201893_x_at	NM_001920	*DCN*	Decorin	0.19	0.039	Proteoglycan involved in matrix assembly
203824_at	NM_004616	*TSPAN8*	Tetraspanin 8	0.17	RVM	Cell surface glycoprotein, integrin binder
204455_at	NM_001723	*DST*	Dystonin	0.14	0.008; RVM	Plakin family protein, hemodesmosomes
201287_s_at	NM_002997	*SDC1*	Syndecan 1	0.12	0.037	Surface proteoglycan, matrix linker, cell spreading and adhesion
201141_at	NM_002510	*GPNMB*	Glycoprotein (transmembrane) nmb, osteoactivin	0.10	0.037; RVM	Type I transmembrane glycoprotein, integrin binding, confers growth delay

Continued on next page

TABLE 1
Continued

Affymetrix ID	Accession	Gene	Gene description	Ratio*	*P* value; RVM†	Molecule/function‡
Morphogenesis/ cytoskeleton organization						
204955_at	NM_006307	*SRPX*	Sushi-repeat-containing protein, X-linked	2.35	0.045	Cytoskeletal association, regulator of cell adhesiveness, proangiogenic
224694_at	NM_032208	*ANTXR1*	Anthrax toxin receptor 1	0.27	0.021; RVM	Type I transmembrane protein, filopodia organization
202890_at	NM_001198608	*MAP7*	Microtubule-associated protein 7	0.26	0.006; RVM	Microtubule-associated protein, cell polarization and differentiation
223687_s_at	NM_017527	*LY6K*	Lymphocyte antigen 6 complex, locus K	0.23	RVM	GPI-anchored membrane protein
206385_at	NM_001149.3	*ANK3*	Ankyrin 3, node of Ranvier (ankyrin G)	0.19	0.043; RVM	Linker protein that anchors cytoskeleton at plasma membrane
205014_at	NM_031308	*EPPK1*	Epiplakin 1	0.16	0.028	Intermediate filament cytolinker
225615_at	NM_001136265	*LOC126917 (IFFO2)*	Intermediate filament family orphan 2	0.16	0.015	Intermediate filament protein
201820_at	NM_000424	*KRT5*	Keratin 5	0.12	RVM	Intermediate filament protein
206276_at	NM_003695	*LY6D*	Lymphocyte antigen 6 complex, locus D	0.09	0.006	Leading edges of filopodia, cell adhesion
Cell-cell adhesion						
205534_at	NM_001173523	*PCDH7*	Protocadherin 7	0.27	0.048; RVM	Member of cadherin superfamily
1569003_at	NM_030938	*TMEM49*	Transmembrane protein 49	0.24	RVM	Membrane protein, induces autophagy of starving cells
226374_at	NM_001338	*CXADR = XCAR*	Coxsackie virus and adenovirus receptor	0.21	0.046	Type 1 membrane protein, homophilic cell adhesion molecule, viral receptor
205595_at	NM_001944	*DSG3*	Desmoglein 3 (pemphigus vulgaris antigen)	0.16	0.049; RVM	Ca-binding transmembrane glycoprotein, vascular integrity
221854_at	AI378979	*PKP1*	Plakophilin 1	0.15	0.002	Member of the arm-repeat (armadillo) and plakophilins, desmosomal protein
206032_at	NM_001941	*DSC3*	Desmocollin 3	0.13	0.032; RVM	Desmosomal protein, cell-cell adhesion
222549_at	NM_021101	*CLDN1*	Claudin 1	0.05	0.005	Ca-independent cell-cell adhesion protein

Continued on facing page

TABLE 1
Continued

Affymetrix ID	Accession	Gene	Gene description	Ratio*	*P* value; RVM†	Molecule/function‡
Cluster C: LEC growth/ lymphangiogenesis						
Response to stimulus/axon guidance						
221933_at	NM_020742	*NLGN4X*	Neuroligin 4, X-linked	4.27	0.025	Neuronal cell surface protein involved in cell junction organization
213194_at	NM_002941	*ROBO1*	Roundabout, axon guidance receptor, homolog 1	0.31	0.007	Ig gene superfamily, axon guidance receptor
204469_at	NM_002851	*PTPRZ1*	Protein tyrosine phosphatase, receptor-type, Z polypeptide 1	0.29	RVM	Receptor protein tyrosine phosphatase, axonogenesis regulation
202391_at	NM_006317	*BASP1*	Brain abundant, membrane attached signal protein 1	0.09	0.021; RVM	Membrane-bound signaling molecule, axon guidance, transcriptional repressor
GPCR signaling						
203096_s_at	BF439282	*RAPGEF2*	Rap guanine nucleotide exchange factor (GEF) 2	3.45	0.011	Ras GTPase activating factor, fosters adherence junction formation
220334_at	NM_012419	*RGS17*	Regulator of G-protein signaling 17	2.63	0.035	GTPase activating protein, inhibitor of GPCR signaling
206701_x_at	NM_000115	*EDNRB*	Endothelin receptor type B	1.76	0.026	GPCR, endothelin signaling
223322_at	BC004270	*RASSF5*	Ras association (RalGDS/AF-6) domain family 5	0.26	0.046	Binder of activated Ras proteins, integrin signaling, directional endothelial cell movement
204803_s_at	NM_004165	*RRAD*	Ras-related associated with diabetes	0.24	RVM	Ras GTPase protein, signal transduction, inhibits vascular lesion formation
229723_at	NM_054114	*TAGAP*	T-cell activation GTPase activating protein	0.21	RVM	ρ GTPase-activating protein
212724_at	BG054844	*RND3*	ρ family GTPase 3	0.12	0.023; RVM	GTP binder, semaphorin signaling in neurons and stress fiber organization
218186_at	NM_020387	*RAB25*	RAB25, member RAS oncogene family	0.11	0.017	Small GTPase protein, control of membrane trafficking, tumor suppressor
Other signaling transduction						
201811_x_at	NM_004844	*SH3BP5*	SH3-domain binding protein 5	1.57	0.023	Protein kinase inhibitor activity
221215_s_at	NM_020639	*RIPK4*	Receptor-interacting serine-threonine kinase 4	0.26	0.043	Protein kinase C–associated kinase
243582_at	NM_152550	*SH3RF2*	SH3 domain containing ring finger 2	0.25	RVM	Negative regulator of phosphatase activities

Continued on next page

TABLE 1
Continued

Affymetrix ID	Accession	Gene	Gene description	Ratio*	*P* value; RVM†	Molecule/function‡
211003_x_at	NM_0040613	*TGM2*	Transglutaminase 2	0.22	RVM	Catalyzer of covalent protein cross-linking, regulation of cell adhesion
226907_at	NM_030949.2	*PPP1R14C*	Protein phosphatase 1, regulatory (inhibitor) subunit 14C	0.13	0.004; RVM	Protein kinase C–enhanced protein phosphatase 1 inhibitor, signaling regulator
Transcriptional regulators						
204689_at	NM_002729	*HHEX*	Hematopoietically expressed homeobox	2.14	0.005	Homeobox transcription factor, regulator of VEGF signaling
201464_x_at	NM_002228	*JUN*	Jun oncogene	1.65	0.018	Virus-derived transcription factor, promotes cell growth, inflammation, etc.
204254_s_at	NM_000376	*VDR*	Vitamin D (1,25-dihydroxyvitamin D3) receptor	0.28	RVM	Nuclear hormone receptor and transcriptional regulator
222895_s_at	NM_138576	*BCL11B*	B-cell CLL/lymphoma 11B	0.25	0.045; RVM	Zn finger protein, proposed tumor suppressor
204653_at	BF343007	*TFAP2A*	Transcription factor AP-2 α	0.25	0.025; RVM	Homo- or heterodimeric transcription factor
221530_s_at	NM_030762	*BHLHB3*	Basic helix-loop-helix domain containing, class B, 3	0.24	0.022; RVM	Transcriptional repressor involved in cell development
205286_at	NM_003222	*TFAP2C*	Transcription factor AP-2 γ (activating enhancer binding protein 2 γ)	0.22	0.014	Homo- or heterodimeric transcription factor, developmentally regulated
202597_at	AU144284	*IRF6*	Interferon regulatory factor 6	0.21	0.021; RVM	Helix-turn-helix transcription factor, negative regulation of proliferation
205251_at	NM_022817	*PER2*	Period homolog 2 (*Drosophila*)	0.20	0.015	Circadian clock gene
209291_at	NM_001546	*ID4* (*BHLHB27*)	Inhibitor of DNA binding 4	0.13	0.049; RVM	Helix-loop-helix transcription factor, repressor of cell proliferation
209212_s_at	AB030824	*KLF5*	Kruppel-like factor 5 (intestinal)	0.13	0.041	Zn finger transcription factor, involved in metabolic regulation
227475_at	AI676059	*FOXQ1*	Forkhead box Q1	0.11	0.035; RVM	Member of *FOX* transcription factors, multiple functions
211597_s_at	AB059408	*HOPX*	HOP homeobox	0.04	0.006	Homeobox transcription factor, tumor suppressor
Cell cycle/mitosis						
212086_x_at	NM_005572	*LMNA*	Lamin A/C	0.50	0.004	Nuclear envelope constituent, associated with lipodystrophy
208079_at	NM_198433	*AURKA*	Aurora kinase A	0.28	RVM	Kinase involved in microtubule formation, mitotic spindle organization

Continued on facing page

TABLE 1
Continued

Affymetrix ID	Accession	Gene	Gene description	Ratio*	*P* value; RVM†	Molecule/function‡
218039_at	NM_016359	*NUSAP1*	Nucleolar and spindle associated protein 1	0.28	RVM	DNA- and microtubule-binding protein, mitotic spindle organization
201291_s_at	NM_001067	*TOP2A*	Topoisomerase II α 170 kDa	0.28	RVM	DNA toposisomerase enzyme, fosters cell cycle progression
202870_s_at	NM_001255	*CDC20*	Cell division cycle 20 homolog	0.27	RVM	Cell cycle control protein, complexes and activates anaphase promoting complex
202756_s_at	NM_002081	*GPC1*	Glypican 1	0.25	0.021	Cell surface heparan sulfate proteoglycan, controlling cell division
222608_s_at	NM_018685	*ANLN*	Anillin	0.22	RVM	Actin-binding protein, controlling cytokinesis in mitosis
230104_s_at	NM_015964	*TPPP3*	Tubulin polymerization-promoting protein family member 3	0.18	0.012	Control of microtubule bundle formation, centrosome amplification
209773_s_at	NM_001165931	*RRM2*	Ribonucleotide reductase M2 polypeptide	0.14	RVM	Redox enzyme catalyzing deoxyribonucleotide synthesis
Cell survival/ apoptosis/p53 signaling						
209863_s_at	AF091627	*TP63*	Tumor protein p63	0.26	RVM	Transcription factor inducing p53 target genes
218499_at	NM_016542	*RP6-213H19.1*	Serine/threonine protein kinase MST4	0.22	0.023; RVM	GCK group III family kinase, cleaved by Casp-3, apoptosis pathway component
202504_at	NM_012101	*TRIM29*	Tripartite motif-containing 29	0.21	0.043; RVM	Transcription factor negatively regulating p53
222392_x_at	AJ251830	*PERP*	PERP, TP53 apoptosis effector	0.17	0.028	p53-regulated desmosomal protein
209569_x_at	NM_014392	*D4S234E* (*P21*)	DNA segment on chromosome 4 (unique) 234 expressed sequence	0.14	0.015	p53-induced proapoptotic protein
206400_at	NM_002307	*LGALS7B*	Lectin, galactoside-binding, soluble, 7 (galectin 7)	0.05	0.005	p53-induced proapoptotic protein
Cluster D: small molecule biochemistry						
Lipid transport/ metabolic process						
220331_at	NM_006668	*CYP46A1*	Cytochrome P450, family 46, subfamily A, polypeptide 1	4.14	0.038	Monooxygenase catalyzing cholesterol turnover and steroid degradation
235978_at	AI766029	*FABP4*	Fatty acid binding protein 4, adipocyte	3.85	RVM	Intracellular free fatty acid chaperone, transcriptional regulator

Continued on next page

TABLE 1
Continued

Affymetrix ID	Accession	Gene	Gene description	Ratio*	*P* value; RVM†	Molecule/function‡
201525_at	NM_001647	*APOD*	Apolipoprotein D	2.64	0.023	Extracellular lipid transport glycoprotein
222217_s_at	NM_024330	*SLC27A3*	Solute carrier family 27 (fatty acid transporter), member 3	2.17	0.007	Transporter of long-chain fatty acids and acyl-CoA activator
205769_at	NM_003645	*SLC27A2*	Solute carrier family 27 (fatty acid transporter), member 2	0.28	RVM	Long-chain fatty acid acyl-CoA ligase
200832_s_at	NM_005063	*SCD-1*	Stearoyl-CoA desaturase	0.23	0.042; RVM	Rate-limiting redox enzyme catalyzing monounsaturated fatty acid biosynthesis
205220_at	NM_006018	*GPR109B*	GPCR 109B	0.07	0.042	Antilipolytic signaling receptor
Glucose transport/ metabolic process						
201250_s_at	NM_006516	*SLC2A1*	Solute carrier family 2 (facilitated glucose transporter), member 1	0.24	RVM	Transmembrane glucose transporter
202934_at	NM_000189	*HK2*	Hexokinase 2	0.17	RVM	Allosteric glucose phosphorylation enzyme during glycolysis
Small molecule transport/ metabolic process						
203473_at	NM_007256	*SLCO2B1*	Solute carrier organic anion transporter family, member 2B1	1.76	0.024	Organic anion and PGE transporter, lipid uptake
224209_s_at	NM_001242505	*GDA*	Guanine deaminase	0.26	RVM	Hydrolytic guanine deamination enzyme
214414_x_at	NM_000558	*HBA1*	Hemoglobin, α 1	0.26	RVM	Hem protein, oxygen transport
209921_at	NM_014331	*SLC7A11*	Solute carrier family 7, (cationic amino acid transporter, y+ system) member 11	0.25	0.036; RVM	Transmembrane transport protein, cysteine:glutamate antiporter activity
217528_at	NM_006536	*CLCA2*	Chloride channel, calcium activated, family member 2	0.21	0.046; RVM	Ca-sensitive chloride conductance protein
204675_at	NM_001047.2	*SRD5A1*	Steroid-5-α-reductase, α polypeptide 1	0.20	0.015; RVM	Steroid degradation redox enzyme
39248_at	NM_004925	*AQP3*	Aquaporin 3	0.17	0.034; RVM	Water and glycerol transport protein
225516_at	NM_003046	*SLC7A2*	Solute carrier family 7, member 2	0.12	RVM	Cationic amino acid transport protein
217564_at	NM_001122633	*CPS1*	Carbamoyl-phosphate synthetase 1	0.10	RVM	Mitochondrial enzyme, removal of excess urea from cells
214164_x_at	NM_001218	*CA12*	Carbonic anhydrase XII	0.07	0.011	Zn metalloenzyme catalyzing hydration of carbon dioxide, acid-base balance
204437_s_at	NM_000802	*FOLR1*	Folate receptor 1	0.04	RVM	5-methyltetrahydrofolate transport protein
217388_s_at	NM_001032998	*KYNU*	Kynureninase	0.02	RVM	Cytoplasmic hydrolase involved in tryptophan metabolism

Continued on facing page

TABLE 1
Continued

Affymetrix ID	Accession	Gene	Gene description	Ratio*	*P* value; RVM†	Molecule/function‡
Unknown						
228977_at	AK090664.1	*LOC729680*	Uncharacterized LOC729680	2.10	<0.001	Unknown
228875_at	NM_001085480.2	*C6orf189 (FAM162B)*	Family with sequence similarity 162, member B	1.90	0.039	Unknown
217966_s_at	NM_052966.2	*FAM129A (GIG39)*	Family with sequence similarity 129, member A	1.85	0.028	Unknown
229518_at	NM_052943.3	*FAM46B*	Family with sequence similarity 46, member B	0.29	0.001; RVM	Unknown
225667_s_at	NM_145175.2	*FAM84A*	Family with sequence similarity 84, member A	0.24	RVM	Unknown
209255_at	NM_014997.3	*KIAA0265 (KLHDC10)*	Kelch domain containing 10	0.27	RVM	Unknown
238063_at	NM_152680.2	*TMEM154*	Transmembrane protein 154	0.24	0.032; RVM	Unknown
212992_at	NM_138420	*C14orf78 (AHNAK2)*	AHNAK nucleoprotein 2	0.23	0.042	Unknown
202503_s_at	NM_014736.4	*KIAA0101*	PCNA associated factor	0.19	RVM	Unknown

APP, amyloid precursor protein; CTSB, cathepsin B; DC, dendritic cell; EGF, epidermal growth factor; GCK, glucokinase gene; GPI, glycophosphatidylinositol; HGF, human growth factor; MHCI, major histocompatibility complex I; PGE, prostaglandin E; RAGE, receptor of advanced glycation end product; ROS, reactive oxygen species; uPA, urokinase. *Shown are ratios of dLECs vs. ndLECs probe set expression. †Statistical significance of the ratio is indicated either as a *P* value of unpaired *t* testing or as a result of RVM analysis, which calculates a probability of genes being found outside of the third SD region (11). ‡Differentially expressed genes were grouped according to their biological functions (gene ontology annotation), and the top differentially expressed genes were ranked in order according to their mean fold change differences.

suppressed by anti-TNF-α antibody (Fig. 6*A*). Because both are involved in the attraction and regulation of leukocyte adhesion and migration to inflamed LECs (20,23), we sought to determine whether they were also relevant for the interaction of macrophages with LECs. TNF-α–treated LEC monolayers showed twofold-enhanced macrophage adhesion in vitro, which could be completely reversed by anti-TNF-α blocking antibody (Fig. 6*B*). Although an anti-VCAM-1 blocking antibody did not interfere with macrophage adhesion to LECs (Fig. 6*C*), inhibitory CXCL10 antibody reduced macrophage adhesion to baseline levels ($P = 0.04$) (Fig. 6*C*), indicating a role of CXCL10 for macrophage interaction with LECs.

LEC-derived CXCL10 is chemotactic for macrophages. To analyze the contribution of LEC-derived CXCL10 to macrophage adhesion, we confirmed enhanced CXCL10 protein levels in LEC lysates and culture supernatants (Supplementary Fig. 8*A* and *B*, respectively) after TNF-α stimulation. Macrophage migration into agarose plugs containing culture supernatants of TNF-α–stimulated LECs showed a twofold increase and could be specifically blocked by inhibitory anti-TNF-α and anti-CXCL10 antibodies (Fig. 6*D*). These data provide evidence for TNF-α–induced CXCL10 secretion of LECs that leads to chemotactic recruitment of macrophages (Fig. 7).

DISCUSSION

Little is currently known about the pathomechanisms of skin manifestations in type 2 diabetes. Here, we aimed to characterize physiological changes of dermal lymphatic vessels by using freshly isolated human LECs. Although thoracic duct and muscle lymphatic vessel alterations were described in diabetic mice (24,25), their skin phenotype has been ignored so far. Analyses of dermal lymphatic functioning, such as lymphangiography, would advance an understanding of disease pathogenesis; however, the single gene defects of these mice have raised doubts about studying impaired diabetic wound healing (26). To our knowledge, this study is among the first (27) to describe morphological and molecular alterations of human dermal lymphatic vessels in type 2 diabetes.

We observed an increased lymphatic vessel density, which was also demonstrated in patients with atherosclerotic lesions (28) and chronic venous insufficiency ulcers (29). In contrast to carcinoma-associated lymphangiogenesis (30), we could not detect laminin and type IV collagen expression alterations, which is consistent with unaltered lymphatic vessel diameter and absence of hyperplasia. We detected reactivated LEC proliferation, as seen by the positive Ki-67 signals in diabetic lymph vessels. This finding was supported by expression changes in p53 target genes and transcription factors implicated in the regulation of proliferation, which might cause a relief of the quiescent state of LECs. Accordingly, p53-deficient mice have shown enhanced lymphangiogenesis (31), and silencing of p53 signaling improved diabetic wound healing as a result of increased lymph vessel generation (32). We traced the downregulation of functionally coherent transcripts such as G-protein–coupled receptor (GPCR) signaling components, p53 effectors, and antiproliferative transcription factors. However, the master regulators dictating the concerted gene suppressions of several gene clusters remain unknown, suggesting involvement of epigenetic, transcriptional, or microRNA-mediated mechanisms. Other findings point toward such regulatory traits in diabetic endothelial cells (33–35). Additionally, enhanced

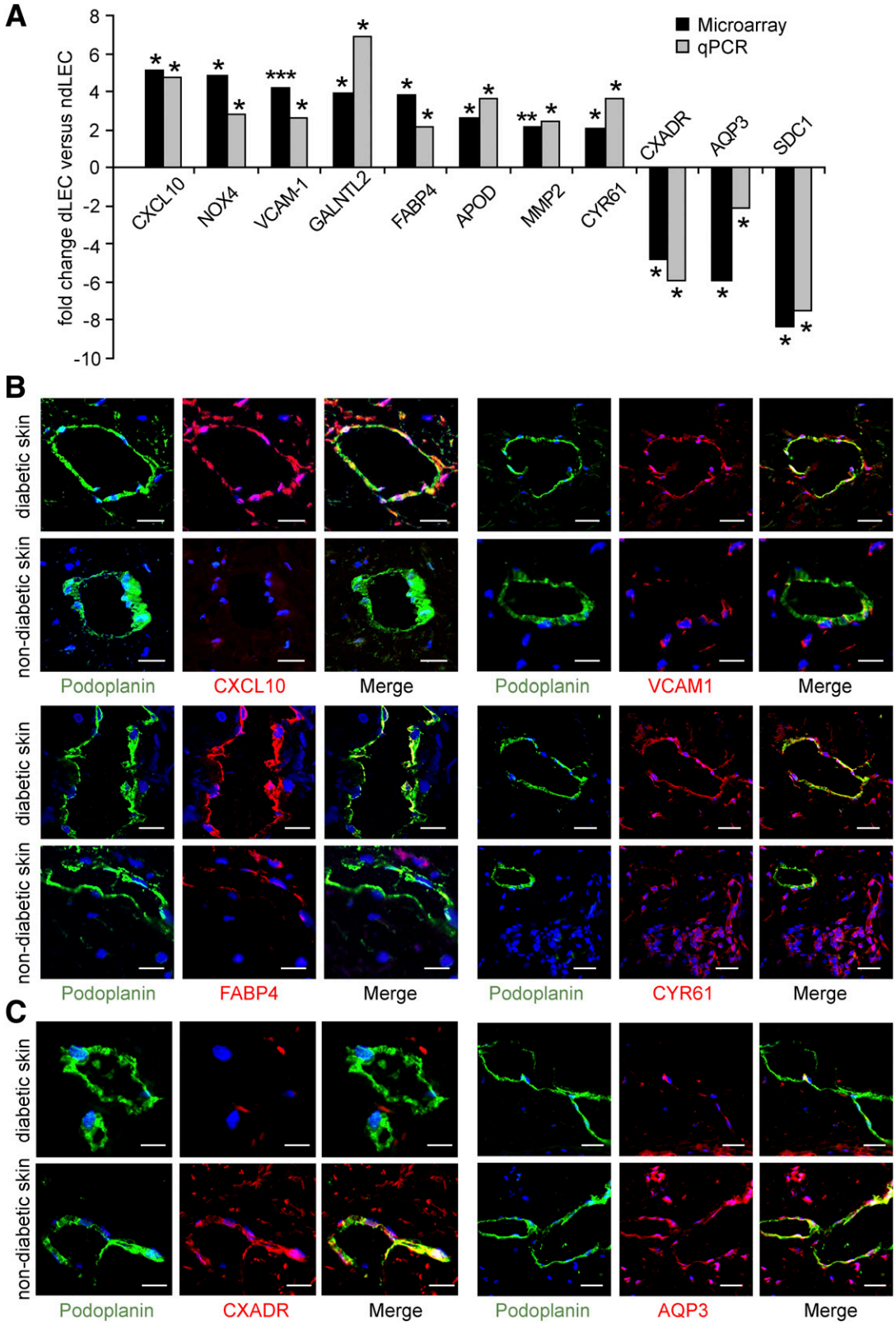

FIG. 3. Confirmation of altered gene expression in lymphatic vessels of type 2 diabetic patients on the mRNA and protein levels. *A*: Representative gene candidates with strong expression change in dLECs vs. ndLECs were selected, and qPCR reactions were performed in triplicate, with total RNA extracted from dLECs and ndLECs (n = 4 in each group) as a template. Fold changes of respective gene expression ratios and statistical significance thereof were calculated and plotted (gray bars) beside the microarray results (black bars) (P values derived from Table 1). *$P < 0.05$; **$P < 0.01$; ***$P < 0.001$. *B* and *C*: Representative images of 5-μm frozen sections of human skin double stained with antipodoplanin and respective antibody to selected candidate genes (n = 4 in each group). Confirmation of enhanced *CXCL10*, *VCAM1*, *FABP4*, and *CYR61* (*B*) and of reduced *CXADR* and *AQP3* (*C*) expression. Scale bars = 20 μm.

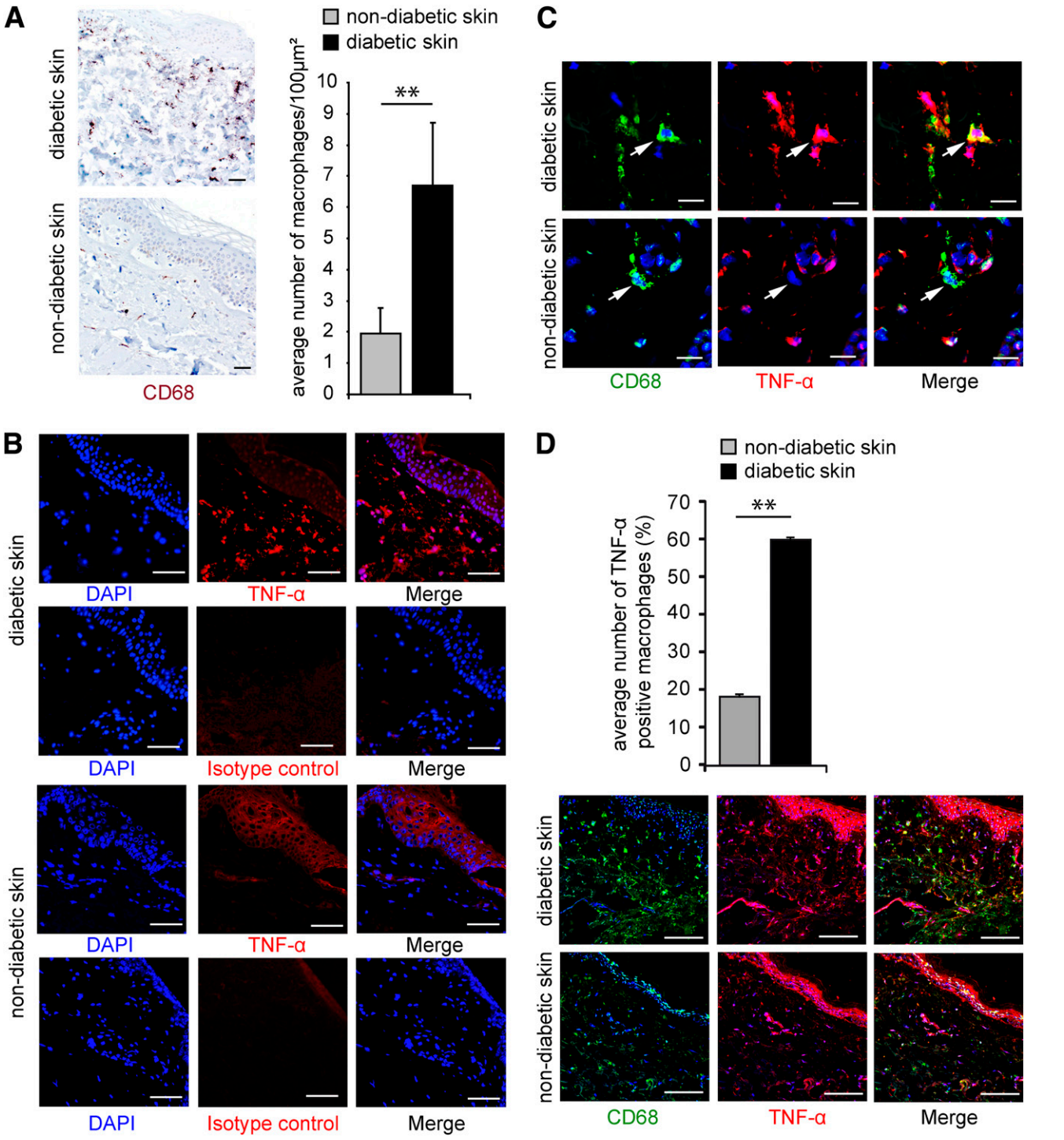

FIG. 4. Enhanced TNF-α levels in human type 2 diabetic skin as a result of macrophage infiltration. *A*: Immunohistochemical evaluation of macrophage infiltration in the skin of type 2 diabetic versus normoglycemic patients. Dermal macrophages were stained with anti-human CD68 antibody. Positive cells were counted per field, and average numbers were calculated per patient group (n = 4 in each group). Scale bars = 100 µm. **$P < 0.001$. *B*: Representative images of immunofluorescence stainings of paraffin skin sections with anti-TNF-α antibody and DAPI as nuclear counterstaining. Although an antibody isotype control showed no reactivity, increased TNF-α staining was detected in type 2 diabetic vs. nondiabetic skin. Scale bars = 100 µm. *C*: Representative images of double immunofluorescence stainings of frozen sections of human type 2 diabetic and nondiabetic skin samples revealing cytoplasmic TNF-α abundance in CD68$^+$ cells. Scale bars: = 20 µm. *D*: Quantitative evaluation of CD68$^+$ macrophages colocalizing with TNF-α in nondiabetic vs. diabetic skin (n = 4 in each group) was performed as described in *A*. Scale bars = 100 µm. **$P = 0.002$.

lymphatic vessel density might be the result of aberrant growth, producing dysfunctional lymph capillaries, and both phenomena might contribute to increased lymph vessel count in the skin of diabetic patients.

The dLEC transcriptome showed neither downregulation of key lymphatic differentiation markers as in obesity and inflammation (36,37) nor deregulation of transcripts for lymphatic valve proteins, although disrupted lymphatic vessel integrity has been postulated to contribute to obesity (38). Rather, overlaps of expression signatures with LECs under hypoxia and from skin of patients with lymphedema (39,40) emphasize a role of these genes in pathologic

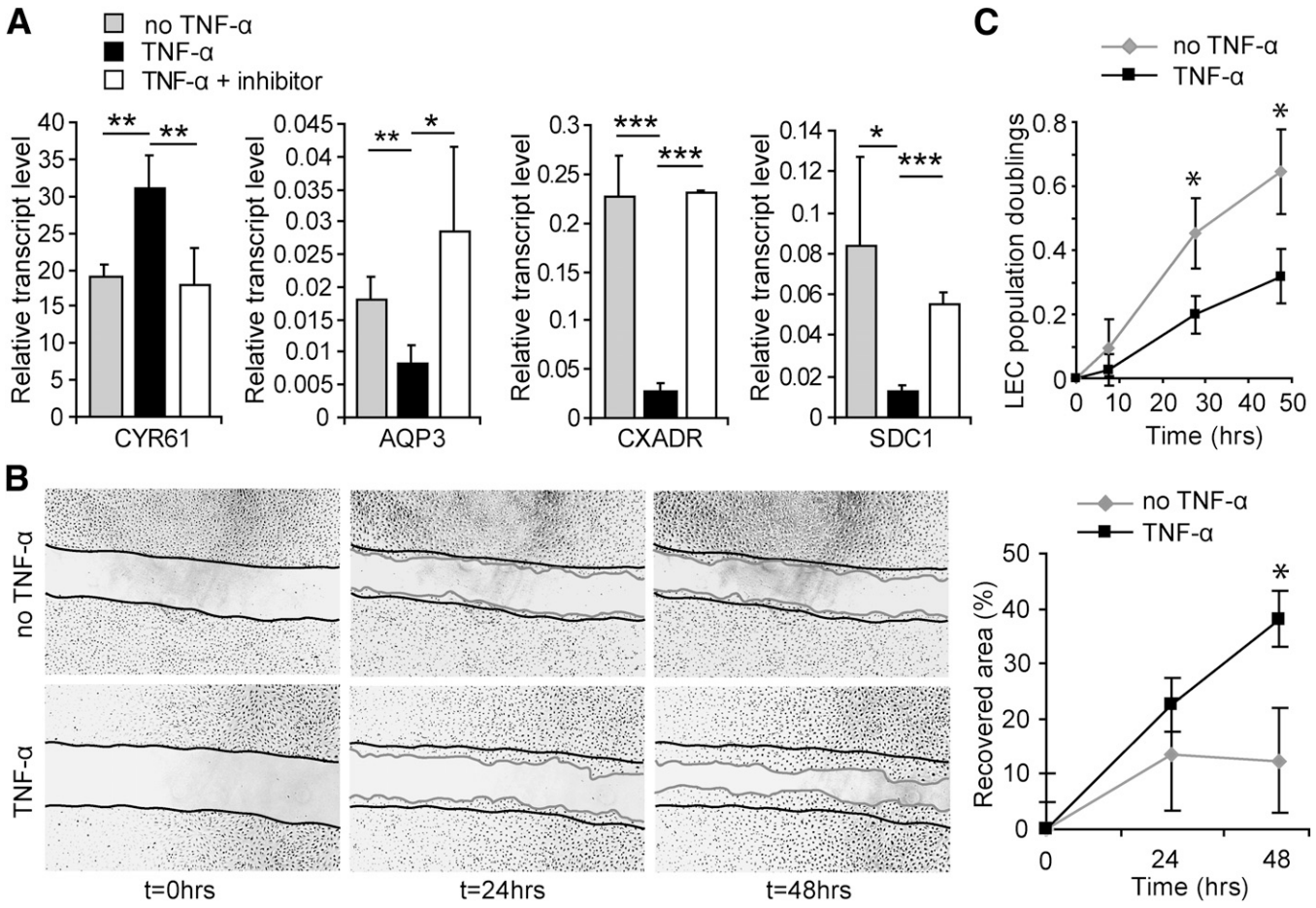

FIG. 5. TNF-α induces altered gene expression involved in a promigratory LEC phenotype in vitro. *A*: qPCR analysis of candidate gene expression in LECs stimulated with TNF-α for 24 h (with or without TNF-α antibody) (n = 3). *P < 0.05; **P < 0.01; ***P < 0.001. *B*: Representative images of an LEC migration assay after creating wounds in LEC monolayers and (n = 3) grown with or without the addition of TNF-α. Reoccupation of the gap by LECs after time (t) = 12 h and t = 48 h (gray line) versus t = 0 h (black line) is seen. The areas repopulated by LECs were measured using AxioVision version 4.7 software, and the percentage of gap area newly covered by LECs was calculated at each time point; *P = 0.007. *C*: LEC doubling rates were reduced under addition of TNF-α. After respective time points, LECs grown in six wells with or without addition of TNF-α were washed, harvested, and counted, and the population doubling was calculated according to ln (cell concentration counted/cell concentration seeded); *P < 0.05. Data are mean ± SD (n = 3 in each group).

lymphatic dysfunction. Furthermore, we observed an overlap with transcriptomes of diabetes complications, such as whole-tissue lysates from nonhealing venous ulcers (41), wound inflammation (42), and diabetic wound microbiome (43), indicating a common diabetes-related gene signature.

Although macrophages are essential for physiological wound healing (44), their increased influx has been correlated with impaired wound healing in type 2 diabetic mice (45), which is characterized by expression of proinflammatory cytokines, especially TNF-α (16). Here, we demonstrate that infiltrating dermal macrophages are a source of TNF-α in human patients as well. We also traced some TNF-α expression in keratinocytes, which has been documented by others (46), but macrophages are supposed to be its predominant source (47). Activated macrophages directly contribute to de novo lymphangiogenesis (18) by *1*) production of lymphangiogenic factors and *2*) conversion into LECs. Pathologic lymphangiogenesis might be driven by additional mediators, such as platelet-derived growth factor-BB, hypoxia-inducible factor, and fibroblast growth factor (FGF) 2 (9), although we did not detect altered expression of these factors or their cognate receptors in dLECs. Rather, we identified a TNF-α responsive set of genes that could be confirmed in vitro, thus excluding indirect effects as a result of LEC cultivation before analysis (10). The TNF-α–induced gene deregulation in human LECs was strongly correlated with a promigratory LEC phenotype, which is in line with enhanced TNF-α levels as a driver of lymph vessel remodeling (48).

In humans, enhanced lymph vessel density correlated with positive disease outcomes (49,50). However, several reports indicated that inflammatory-driven lymphangiogenesis leads to dysfunctional vessel formation with reduced lymph drainage capacity (9). Macrophage recruitment to dLECs through CXCL10 chemotaxis might be indicative of such impeded clearance but could also be a prerequisite to lymph vessel integration. In a lipopolysaccharide-driven peritonitis model, increased numbers of macrophages were closely attached to newly formed inflammatory lymphatic vessels, directly incorporating into these (51). It is tempting to speculate that human skin macrophages are involved in an analog manner of lymph vessel expansion. Aberrantly grown lymphatic vessels could lead to decreased tissue fluid, lipid and immune cell drainage, and finally, persistent inflammation that all together hinder skin regeneration. The

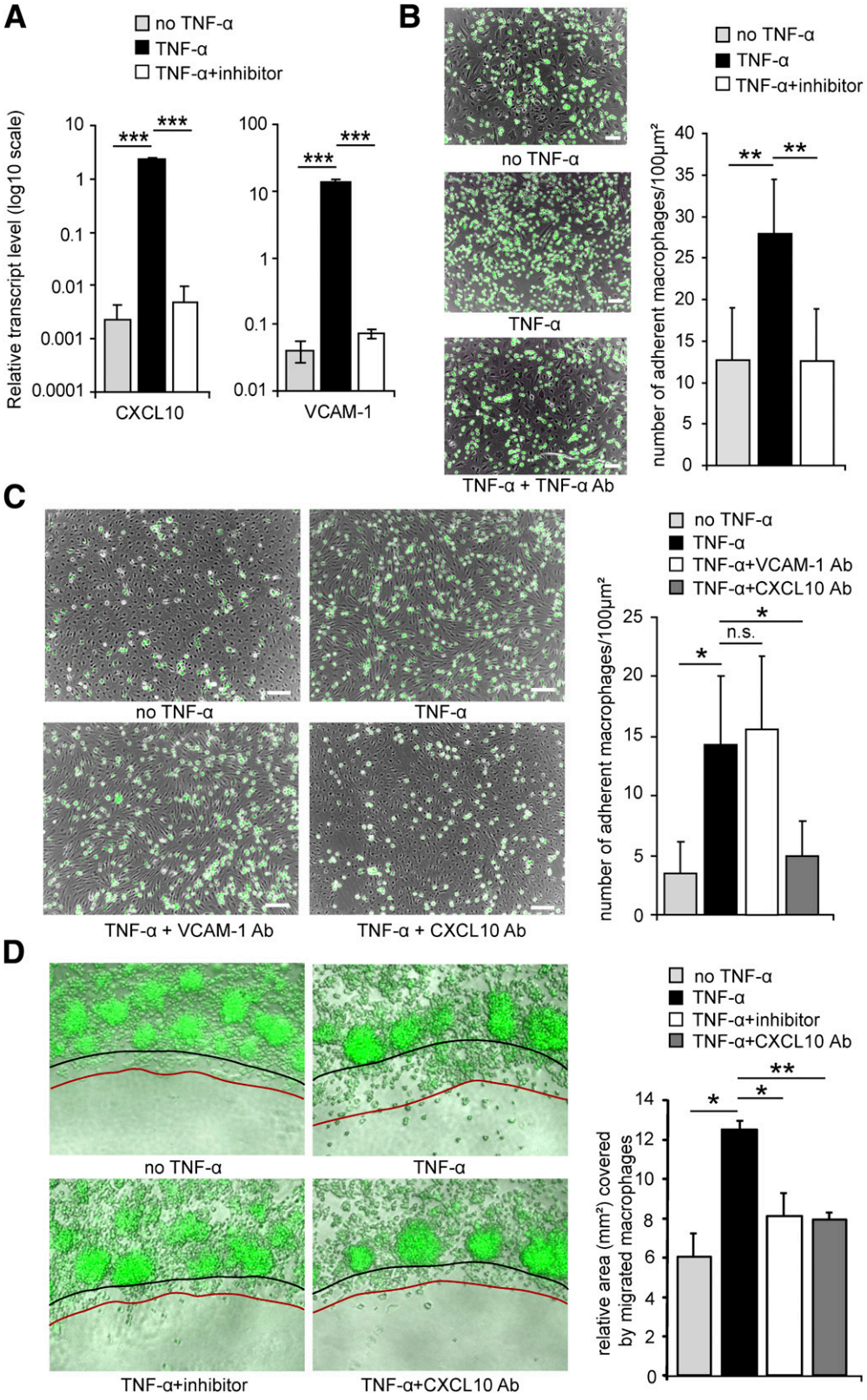

FIG. 6. TNF-α induces altered macrophage adhesion to LECs through CXCL10 secretion in vitro. *A*: Quantitative real-time PCR analysis of *CXCL10* and *VCAM1* expression in human dermal LECs stimulated with TNF-α for 24 h (with or without TNF-α antibody [Ab]). ***$P < 0.001$. *B*: Representative images of macrophage adhesion assays and quantitative evaluation thereof. CellTracker Green–labeled and PMA-stimulated THP-1 cells were added to LEC monolayers ($n = 3$) treated without or with TNF-α and with anti-TNF-α Ab. Macrophages showed enhanced adhesion to TNF-α–treated LEC monolayers, which was blocked by anti-TNF-α Ab. Scale bars = 100 μm. **$P < 0.01$. *C*: CellTracker Green–labeled and PMA-stimulated THP-1 cells were added to LEC monolayers ($n = 3$) treated without and with TNF-α, and with anti-VCAM-1 Ab and anti-CXCL10 Ab, and adhesion was assessed as described previously. Scale bars = 100 μm. *$P < 0.05$. *D*: CXCL10 secreted by LECs is chemotactic to macrophages. Representative images of an agarose migration assay performed in triplicate and its quantitative evaluation. Migration of CellTracker Green–labeled THP-1 cells (*top*) into the agarose spot (*bottom*) after 48 h (red line) vs. 0 h (black line) is seen. Macrophage chemotaxis was enhanced toward agarose spots containing supernatants of TNF-α–stimulated LECs and was inhibited by TNF-α–blocking and CXCL10-blocking Ab. *$P < 0.05$; **$P < 0.01$. NS, not significant.

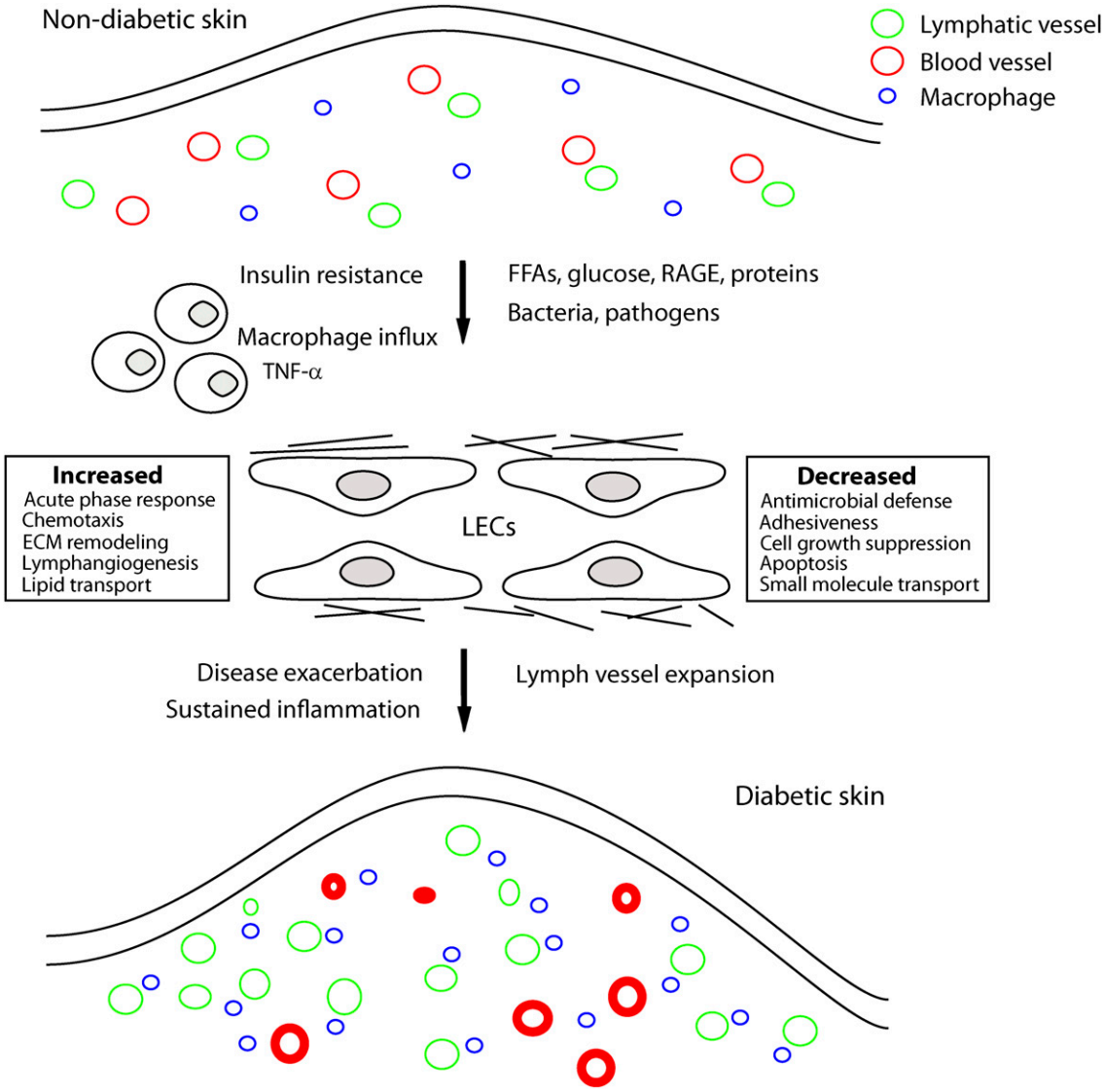

FIG. 7. A cascade of pathogenic events may lead to lymphatic vascular reorganization in type 2 diabetic skin. Increased load of metabolites and macrophage influx over time might lead to molecular alterations in dermal LECs. Hence, dLECs reveal an activated phenotype characterized by increased inflammatory, migratory, and lymphangiogenic status and apoptosis resistance. This lymph vessel phenotype may contribute to chronic inflammation, decreased defense against infections, leukocyte recruitment, tissue remodeling, and severely altered skin homeostasis. Specifically, TNF-α is a key mediator of cross talk between proinflammatory macrophages and LECs. TNF-α–mediated gene expression alterations in dLECs may lead to further macrophage recruitment, reinforcing lymph vessel expansion and chronic inflammation. RAGE, receptor of advanced glycation end product.

question of whether exaggerated lymph vessel formation is beneficial for type 2 diabetes skin pathology must be explored.

ACKNOWLEDGMENTS

M.H. and T.K. were funded within the PhD-CCHD (Cell Communication in Health and Disease) program (http://www.meduniwien.ac.at/phd-cchd) supported by the Austrian Science Fund (FWF project no. W1205). G.E. was supported by an Elise Richter Fellowship (FWF V102-B12) and an FP7 Marie Curie International Reintegration grant (IRG230984).

No potential conflicts of interest relevant to this article were reported.

M.H. performed research, analyzed data, and wrote the manuscript. T.K. performed research and analyzed data. G.E. researched data and reviewed and edited the manuscript. H.S., C.W.S., and M.K.B. performed research. D.S. researched data. C.N. provided human skin material and clinical data and contributed to the discussion. D.K. conceived the project and reviewed and edited the manuscript. B.H. designed the research, analyzed data, and wrote the manuscript. B.H. is the guarantor of this work and, as such, had full access to all the data in the study and takes responsibility for the integrity of the data and the accuracy of the data analysis.

The authors thank Dr. Daniela Haluza, Institute of Environmental Health, Medical University of Vienna (MUW), and Romana Kalt and Ingrid Raab, Clinical Institute of Pathology, MUW, for excellent technical assistance. The authors also thank Dr. Martin Bilban, Department of Laboratory Medicine, MUW, for help with biostatistics; and Dr. Maximilian Zeyda, Department of Internal Medicine, MUW, and Dr. Andrew Rees and Dr. Georg Krupitza, Clinical Institute of Pathology, MUW, for helpful discussions.

REFERENCES

1. Wild S, Roglic G, Green A, Sicree R, King H. Global prevalence of diabetes: estimates for the year 2000 and projections for 2030. Diabetes Care 2004; 27:1047–1053
2. Stumvoll M, Goldstein BJ, van Haeften TW. Type 2 diabetes: principles of pathogenesis and therapy. Lancet 2005;365:1333–1346
3. Shoelson SE, Lee J, Goldfine AB. Inflammation and insulin resistance. J Clin Invest 2006;116:1793–1801
4. O'Rahilly S. Human genetics illuminates the paths to metabolic disease. Nature 2009;462:307–314
5. Hermans MP. Diabetes and the endothelium. Acta Clin Belg 2007;62:97–101
6. Van Hattem S, Bootsma AH, Thio HB. Skin manifestations of diabetes. Cleve Clin J Med 2008;75:772, 774, 776–777 passim
7. Jansson P-A. Endothelial dysfunction in insulin resistance and type 2 diabetes. J Intern Med 2007;262:173–183
8. Wang Y, Oliver G. Current views on the function of the lymphatic vasculature in health and disease. Genes Dev 2010;24:2115–2126
9. Alitalo K. The lymphatic vasculature in disease. Nat Med 2011;17:1371–1380
10. Wick N, Saharinen P, Saharinen J, et al. Transcriptomal comparison of human dermal lymphatic endothelial cells ex vivo and in vitro. Physiol Genomics 2007;28:179–192
11. Stokic D, Wick N, Biely C, Gurnhofer E, Thurner S. Statistically consistent identification of differentially expressed genes in DNA chip data over the whole expression range: relative variance method. Appl Bioinformatics 2006;5:277–284
12. Wiggins H, Rappoport J. An agarose spot assay for chemotactic invasion. Biotechniques 2010;48:121–124
13. Middleton J, Americh L, Gayon R, et al. A comparative study of endothelial cell markers expressed in chronically inflamed human tissues: MECA-79, Duffy antigen receptor for chemokines, von Willebrand factor, CD31, CD34, CD105 and CD146. J Pathol 2005;206:260–268
14. Wick N, Haluza D, Gurnhofer E, et al. Lymphatic precollectors contain a novel, specialized subpopulation of podoplanin low, CCL27-expressing lymphatic endothelial cells. Am J Pathol 2008;173:1202–1209
15. Podgrabinska S, Braun P, Velasco P, Kloos B, Pepper MS, Skobe M. Molecular characterization of lymphatic endothelial cells. Proc Natl Acad Sci U S A 2002;99:16069–16074
16. Khanna S, Biswas S, Shang Y, et al. Macrophage dysfunction impairs resolution of inflammation in the wounds of diabetic mice. PLoS ONE 2010;5: e9539
17. Hotamisligil GS, Shargill NS, Spiegelman BM. Adipose expression of tumor necrosis factor-alpha: direct role in obesity-linked insulin resistance. Science 1993;259:87–91
18. Kerjaschki D. The crucial role of macrophages in lymphangiogenesis. J Clin Invest 2005;115:2316–2319
19. Kainulainen V, Nelimarkka L, Järveläinen H, Laato M, Jalkanen M, Elenius K. Suppression of syndecan-1 expression in endothelial cells by tumor necrosis factor-alpha. J Biol Chem 1996;271:18759–18766
20. Johnson LA, Clasper S, Holt AP, Lalor PF, Baban D, Jackson DG. An inflammation-induced mechanism for leukocyte transmigration across lymphatic vessel endothelium. J Exp Med 2006;203:2763–2777
21. Leu S-J, Lam SC-T, Lau LF. Pro-angiogenic activities of CYR61 (CCN1) mediated through integrins alphavbeta3 and alpha6beta1 in human umbilical vein endothelial cells. J Biol Chem 2002;277:46248–46255
22. Mirza M, Pang MF, Zaini MA, et al. Essential role of the coxsackie- and adenovirus receptor (CAR) in development of the lymphatic system in mice. PLoS ONE 2012;7:e37523
23. Dufour JH, Dziejman M, Liu MT, Leung JH, Lane TE, Luster AD. IFN-gamma-inducible protein 10 (IP-10; CXCL10)-deficient mice reveal a role for IP-10 in effector T cell generation and trafficking. J Immunol 2002;168: 3195–3204
24. Moriguchi P, Sannomiya P, Lara PF, Oliveira-Filho RM, Greco KV, Sudo-Hayashi LS. Lymphatic system changes in diabetes mellitus: role of insulin and hyperglycemia. Diabetes Metab Res Rev 2005;21:150–157
25. Kivelä R, Silvennoinen M, Lehti M, Kainulainen H, Vihko V. Effects of acute exercise, exercise training, and diabetes on the expression of lymphangiogenic growth factors and lymphatic vessels in skeletal muscle. Am J Physiol Heart Circ Physiol 2007;293:H2573–H2579
26. Plum L, Wunderlich FT, Baudler S, Krone W, Brüning JC. Transgenic and knockout mice in diabetes research: novel insights into pathophysiology, limitations, and perspectives. Physiology (Bethesda) 2005;20:152–161
27. Kaufmann A, Molnár B, Craciun C, Itcus A. Diabetic lymphangiopathy. An optical and electron microscopic study. Lymphology 1980;13:202–206
28. Kholová I, Dragneva G, Cermáková P, et al. Lymphatic vasculature is increased in heart valves, ischaemic and inflamed hearts and in cholesterol-rich and calcified atherosclerotic lesions. Eur J Clin Invest 2011;41:487–497
29. Fernandez AP, Mitiva M, Roberts B, Ricotti C, Rouhani P, Romanelli P. Histopathologic analysis of dermal lymphatic alterations in chronic venous insufficiency ulcers using D2-40. J Am Acad Dermatol 2011;64:1123.e1–12
30. Vainionpää N, Bützow R, Hukkanen M, et al. Basement membrane protein distribution in LYVE-1-immunoreactive lymphatic vessels of normal tissues and ovarian carcinomas. Cell Tissue Res 2007;328:317–328
31. Ruddell A, Kelly-Spratt KS, Furuya M, Parghi SS, Kemp CJ. p19/Arf and p53 suppress sentinel lymph node lymphangiogenesis and carcinoma metastasis. Oncogene 2008;27:3145–3155
32. Nguyen PD, Tutela JP, Thanik VD, et al. Improved diabetic wound healing through topical silencing of p53 is associated with augmented vasculogenic mediators. Wound Repair Regen 2010;18:553–559
33. Pirola L, Balcerczyk A, Tothill RW, et al. Genome-wide analysis distinguishes hyperglycemia regulated epigenetic signatures of primary vascular cells. Genome Res 2011;21:1601–1615
34. Cayrol C, Lacroix C, Mathe C, et al. The THAP-zinc finger protein THAP1 regulates endothelial cell proliferation through modulation of pRB/E2F cell-cycle target genes. Blood 2007;109:584–594
35. Zampetaki A, Kiechl S, Drozdov I, et al. Plasma microRNA profiling reveals loss of endothelial miR-126 and other microRNAs in type 2 diabetes. Circ Res 2010;107:810–817
36. Horra A, Salazar J, Ferré R, et al. Prox-1 and FOXC2 gene expression in adipose tissue: a potential contributory role of the lymphatic system to familial combined hyperlipidaemia. Atherosclerosis 2009;206:343–345
37. Vigl B, Aebischer D, Nitschké M, et al. Tissue inflammation modulates gene expression of lymphatic endothelial cells and dendritic cell migration in a stimulus-dependent manner. Blood 2011;118:205–215
38. Harvey NL, Srinivasan RS, Dillard ME, et al. Lymphatic vascular defects promoted by Prox1 haploinsufficiency cause adult-onset obesity. Nat Genet 2005;37:1072–1081
39. Irigoyen M, Ansó E, Martínez E, Garayoa M, Martínez-Irujo JJ, Rouzaut A. Hypoxia alters the adhesive properties of lymphatic endothelial cells. A transcriptional and functional study. Biochim Biophys Acta 2007;1773: 880–890
40. Ogunbiyi S, Chinien G, Field D, et al; London Lymphedema Consortium. Molecular characterization of dermal lymphatic endothelial cells from primary lymphedema skin. Lymphat Res Biol 2011;9:19–30
41. Charles CA, Tomic-Canic M, Vincek V, et al. A gene signature of non-healing venous ulcers: potential diagnostic markers. J Am Acad Dermatol 2008;59:758–771
42. Roy S, Khanna S, Rink C, Biswas S, Sen CK. Characterization of the acute temporal changes in excisional murine cutaneous wound inflammation by screening of the wound-edge transcriptome. Physiol Genomics 2008;34:162–184
43. Grice EA, Snitkin ES, Yockey LJ, Bermudez DM, Liechty KW, Segre JA; NISC Comparative Sequencing Program. Longitudinal shift in diabetic wound microbiota correlates with prolonged skin defense response. Proc Natl Acad Sci U S A 2010;107:14799–14804
44. Mahdavian Delavary B, van der Veer WM, van Egmond M, Niessen FB, Beelen RH. Macrophages in skin injury and repair. Immunobiology 2011; 216:753–762
45. Wetzler C, Kämpfer H, Stallmeyer B, Pfeilschifter J, Frank S. Large and sustained induction of chemokines during impaired wound healing in the genetically diabetic mouse: prolonged persistence of neutrophils and macrophages during the late phase of repair. J Invest Dermatol 2000;115:245–253
46. Brandner JM, Zacheja S, Houdek P, Moll I, Lobmann R. Expression of matrix metalloproteinases, cytokines, and connexins in diabetic and nondiabetic human keratinocytes before and after transplantation into an ex vivo wound-healing model. Diabetes Care 2008;31:114–120
47. Barrientos S, Stojadinovic O, Golinko MS, Brem H, Tomic-Canic M. Growth factors and cytokines in wound healing. Wound Repair Regen 2008;16:585–601
48. Baluk P, Yao LC, Feng J, et al. TNF-alpha drives remodeling of blood vessels and lymphatics in sustained airway inflammation in mice. J Clin Invest 2009;119:2954–2964
49. Labanaris AP, Polykandriotis E, Horch RE. The effect of vacuum-assisted closure on lymph vessels in chronic wounds. J Plast Reconstr Aesthet Surg 2009;62:1068–1075
50. von der Weid PY, Rehal S, Ferraz JG. Role of the lymphatic system in the pathogenesis of Crohn's disease. Curr Opin Gastroenterol 2011;27:335–341
51. Kim KE, Koh YJ, Jeon BH, et al. Role of CD11b+ macrophages in intraperitoneal lipopolysaccharide-induced aberrant lymphangiogenesis and lymphatic function in the diaphragm. Am J Pathol 2009;175:1733–1745